

Revised Version 1999
Theoretical Physics Seminar
in Trondheim No 6 1998

Quantum Dynamics of Non-Degenerate Parametric Amplification

Per K. Rekdal^{1,a} and Bo-Sture K. Skagerstam^{2,a,b}

^{a)}Department of Physics, The Norwegian University of Science and Technology,
N-7491 Trondheim, Norway

^{b)}Theoretical Physics Division, CERN, CH-1211, Geneva 23, Switzerland

Physica Scripta (in press)

Abstract

A simple model of a two-mode non-resonant parametric amplifier is studied with special regard to non-classical features such as revivals and squeezing. The methods used apply for an arbitrary pump parameter. Detailed analytical and explicit expressions are given when the coupling of the two modes has an harmonic time-dependence. Despite its simplicity the model exhibits a very broad range of intricate physical effects. We show that quantum revivals are possible for a broad continuous range of physical parameters in the case of initial Fock states. For coherent states we find that such revivals are possible only for certain discrete rational number combinations of the ratio of frequency detuning and pump parameters. Correlation effects are shown to be very sensitive to the initial state of the system.

¹Email address: perr@phys.ntnu.no.

²Email address: boskag@phys.ntnu.no.

1 Introduction

The quantum-mechanical analysis of coupled harmonic oscillators enters into many fields of physics. In the design of detectors for gravitational radiation the dynamics of an harmonic oscillator and a transducer is e.g. of importance (see e.g. Ref.[1]). The coupling of free quantum fields to classical external fields can also be thought of as a system of harmonic oscillators with, in general, space- and time-dependent couplings (see e.g. Ref.[2]). In the field of quantum optics similar systems of coupled harmonic oscillator systems are of great interest as e.g. in the description of parametric down-conversion of photons (see e.g. Refs.[3, 4, 5, 6, 7, 8, 9, 10, 11, 12]).

Our primary goal here is to study a simple interaction between a LC-circuit and one mode of the second quantized radiation field all without damping effects included. The corresponding free Hamiltonians are used to define reference states as e.g. the notion of a photon. In order to calculate photon-number distributions at any time normal ordering procedures become an essential ingredient in our study. In particular we have, in terms of a canonical rescaling of variables, considered the following classical Hamiltonian

$$H = \frac{1}{2}P_a^2 + \frac{1}{2}\omega_a^2Q_a^2 + \frac{1}{2}P_b^2 + \frac{1}{2}\omega_b^2Q_b^2 - g \left(\sqrt{\frac{\omega_a}{\omega_b}}Q_aP_b + \sqrt{\frac{\omega_b}{\omega_a}}P_aQ_b \right) , \quad (1)$$

where the canonical momentum P_a is proportional to the electric current $I = dQ_a/dt$ of the LC-circuit with inductance L and capacitance C ($\omega_a = 1/\sqrt{LC}$). P_b and Q_b describe the harmonic oscillator of the singe-mode of the radiation field with frequency ω_b . The last interaction term is a simple form for the interaction of the radiation-field with the LC-circuit in terms of a real coupling constant g . The particular form of the interaction term in Eq. (1) is motivated by the fact that a minor extension of this model can also be used to describe non-resonant parametric down-conversion, as will be discussed in more detail Section 2. Eq. (1) is also the Hamiltonian for a two-dimensional electrically charged harmonic oscillator, in general non-isotropic, with an external magnetic field $B = g(\sqrt{\omega_b/\omega_a} - \sqrt{\omega_a/\omega_b})$ perpendicular to the ab-plane and with angular frequencies $\omega_a^2 \rightarrow \omega_a^2 - g^2\omega_b/\omega_a$ and $\omega_b^2 \rightarrow \omega_b^2 - g^2\omega_a/\omega_b$. If the original angular frequencies ω_a and ω_b are equal the harmonic oscillator becomes isotropic and the magnetic field is zero.

Despite the very simple structure of the Hamiltonian Eq. (1) we will see that the corresponding quantum dynamics can lead to quite intriguing physics. In view of the impressive experimental developments in quantum optics the system under consideration may actually be realized in the laboratory.

The paper is organized as follows. In Section 2 the dynamical system is defined in more detail. An exact treatment of the time-evolution operator is presented in Section 3. The results obtained turn out to have a broad range of applicability. Quantum revivals and their dependence of initial states are discussed in Section 4. In Section 5 non-classical features are studied in terms of correlation functions. The effect of detuning on the squeezing properties of a parametric amplifier is studied in Section 6. Signal-to-noise aspects are discussed in Section 7 and some final remarks are given in Section 8.

2 The Dynamical System

The coupled harmonic oscillators we consider are described by the two-mode Hamiltonian

$$H = H_a + H_b + H_{int} \quad , \quad (2)$$

where

$$\begin{aligned} H_a &= \omega_a(n_a + \frac{1}{2}) \quad , \\ H_b &= \omega_b(n_b + \frac{1}{2}) \quad , \end{aligned} \quad (3)$$

in natural units ($\hbar = c = 1$) and where $n_a \equiv a^\dagger a$ and $n_b \equiv b^\dagger b$. The interaction between the a and b mode is chosen to be of the form

$$H_{int} = i [g(t) ab - g^*(t) a^\dagger b^\dagger] \quad , \quad (4)$$

where $g(t)$ is a time-dependent coupling. If $g(t) = g$ we recover the system described by Eq. (1). The interaction Hamiltonian Eq. (4) describes a two-mode non-degenerate parametric down-conversion process, where the modes are known as “signal” and “idler” and where the pump parameter $g(t)$ then describes an arbitrary classical pump field (for reviews see e.g. Refs.[11, 13, 14, 15, 16]).

The Hamiltonian (4) can be written in the form

$$H_{int} = i [g(t)K_- - g^*(t)K_+] \quad , \quad (5)$$

where

$$K_- \equiv ab \quad , \quad K_+ \equiv a^\dagger b^\dagger \quad , \quad K_0 \equiv \frac{a^\dagger a + b b^\dagger}{2} \quad , \quad (6)$$

span the Lie algebra of the non-compact group $SU(1, 1)$, i.e.

$$[K_+, K_-] = -2K_0 \quad , \quad [K_0, K_\pm] = \pm K_\pm \quad . \quad (7)$$

The Casimir operator of the Lie-algebra Eq. (7) is given by $C = K_0^2 - K_+K_- - K_0 = \Phi(\Phi + 1)$, where we can choose $-2\Phi = |n_a - n_b| + 1$. We therefore see that we have a realization of the unitary representation $D^+(\Phi)$ of $SU(1, 1)$ [17]. We observe that when we make the identification $a = b$, the Hamiltonian describes a *degenerate* parametric amplifier. This corresponds to a realization of the $SU(1, 1)$ Lie-algebra Eq. (7) with $K_- = a^2/2$, $K_+ = (a^\dagger)^2/2$ and $K_0 = (a^\dagger a + aa^\dagger)/4$ which also constitutes a realization of a discrete unitary representation of $SU(1, 1)$ [19].

3 The Time-Evolution Operator

The Hamiltonian in the interaction picture and in terms of the operators K_+ and K_- reads

$$H_{int}^I(t) = i [g(t)e^{-i(\omega_a + \omega_b)t}K_- - g^*(t)e^{i(\omega_a + \omega_b)t}K_+] \quad , \quad (8)$$

with the corresponding Schrödinger equation

$$i \frac{d}{dt} U_I(t) = i [\tilde{g}(t)K_- - \tilde{g}^*(t)K_+] U_I(t) \quad , \quad (9)$$

and where we have defined $\tilde{g}(t) \equiv g(t)e^{-i(\omega_a + \omega_b)t}$. An exact analytical expression for the time-evolution operator $U_I(t)$ can be obtained as follows. Due to the presence of the Lie-algebra of $SU(1, 1)$ we employ the Wei-Norman technique [18, 19] and express the time-evolution operator in the following form

$$U_I(t) = e^{A_+(t)K_+} e^{2A_0(t)K_0} e^{A_-(t)K_-} \quad , \quad (10)$$

since this is a convenient choice when computing expectation values and probability amplitudes. If we substitute Eq. (10) into the Schrödinger equation Eq. (9) we find that $A_+(t)$, $A_-(t)$ and $A_0(t)$ must satisfy the following system of non-linear differential equations:

$$\begin{aligned} \frac{d}{dt} A_+(t) &= \tilde{g}(t)A_+^2(t) - \tilde{g}^*(t) \quad , \\ \frac{d}{dt} A_0(t) &= \tilde{g}(t)A_+(t) \quad , \end{aligned} \quad (11)$$

$$\frac{d}{dt}A_-(t) = \tilde{g}(t)e^{2A_0(t)} ,$$

with the initial conditions $A_+(0) = A_-(0) = A_0(0) = 0$. These initial conditions ensure that $U_I(0) = 1$. Eqs. (11) are actually valid for the Hamiltonian Eq.(4) in general and can e.g. be studied by making use of various numerical methods. In the present paper we will, however, consider a simple situation in which case analytical methods are at hand, i.e. we consider a coupling $g(t)$ with harmonic time-dependence

$$g(t) = ge^{i\omega t} , \quad (12)$$

where g is a real constant. For parametric down-conversion processes the frequency ω is then referred to as the pump frequency. In the course of preparation of the present paper we have observed that in the special case of the time-dependence of Eq. (12) algebraic methods can be used to solve for Eq. (9) (see e.g. Ref.[20]). To the extent one can compare our methods and results with those of Ref.[20] we find agreement. We, however, once more stress that our methods in principle can be used for an arbitrary time-dependence of $g(t)$. It is convenient to define

$$\Omega = \omega - \omega_a - \omega_b . \quad (13)$$

When the frequencies ω_a and ω_b sum up to the classical pump frequency ω , i.e. $\Omega = 0$, we have parametric resonance. In this case the Schrödinger equation is easy to solve (see e.g. Ref. [14]).

Let us now consider the more general situation $\Omega \neq 0$, in which case the interaction Hamiltonian constitutes a simple model of a detuned "broad-band" pump in parametric amplification. Within first-order perturbation theory, in which case the time-ordering procedure of the time-evolution operator is not important, the broad-band pump down-conversion has been considered in great detail in the literature [21, 22, 23, 24, 25, 26, 27, 28, 29]. Here we are interested in an exact treatment of the time-evolution operator, i.e. we have to solve Eqs. (11) with the harmonic time-dependence Eq. (12). An exact treatment can, e.g., be used to investigate unitarity effects (i.e. including not only the vacuum and the two-photon states but all possible intermediate states) of photon correlation experiments.

A important point here is that we have to solve Eqs. (11) separately for three different cases: $k^2 < 1$, $k^2 > 1$ and $k^2 = 1$, where we have defined the dimensionless parameter

$$k \equiv \frac{\Omega}{2g} . \quad (14)$$

In the case $k^2 < 1$, the solution has the form

$$\begin{aligned} A_+(t) &= -e^{-i\Omega t} \left[\sqrt{1-k^2} \tanh \left(gt\sqrt{1-k^2} - i\gamma \right) + ik \right] , \\ A_-(t) &= \sqrt{1-k^2} \tanh \left(gt\sqrt{1-k^2} - i\gamma \right) + ik , \\ A_0(t) &= -\ln \left[\frac{\cosh (gt\sqrt{1-k^2} - i\gamma)}{\cos \gamma} \right] - \frac{i\Omega}{2}t , \end{aligned} \quad (15)$$

where

$$\tan \gamma = \frac{k}{\sqrt{1-k^2}} . \quad (16)$$

The solution in the case $k^2 > 1$ is of the same form as in the case above with the substitutions $\gamma \rightarrow -\gamma (\equiv \delta)$, $\tanh \rightarrow \cot$ and $\cos \rightarrow i \sinh$. The explicit solution of the Eqs. (11) is then

$$\begin{aligned} A_+(t) &= -e^{-i\Omega t} \left[\sqrt{k^2-1} \cot \left(gt\sqrt{k^2-1} + i\delta \right) + ik \right] , \\ A_-(t) &= \sqrt{k^2-1} \cot \left(gt\sqrt{k^2-1} + i\delta \right) + ik , \\ A_0(t) &= -\ln \left[\frac{\sin (gt\sqrt{k^2-1} + i\delta)}{\sin(i\delta)} \right] - \frac{i\Omega}{2}t , \end{aligned} \quad (17)$$

where now

$$\coth \delta = \frac{k}{\sqrt{k^2-1}} . \quad (18)$$

If $k^2 = 1$ it is particularly easy to show that

$$\begin{aligned} A_+(t) &= -e^{-i\Omega t} \left[\frac{1}{gt+i} + i \right] , \\ A_-(t) &= \left[\frac{1}{gt+i} + i \right] , \\ A_0(t) &= -\ln [1 - igt] - \frac{i\Omega}{2}t , \end{aligned} \quad (19)$$

is the solution of the Eqs. (11) with the correct initial conditions. We notice that $A_+(t) = -e^{-i\Omega t} A_-(t)$ for all three cases.

Due to the constraint of unitarity, i.e. $U_I^\dagger(t) = U_I^{-1}(t)$, the functions $A_+(t)$, $A_-(t)$ and $A_0(t)$ are not independent. By making use of operator reordering techniques (for a

pedagogical account see e.g. Ref.[30]), the unitarity of $U_I(t)$ leads to the general conditions

$$\begin{aligned} A_+^*(t) &= -\frac{A_-(t)}{e^{2A_0(t)} - A_-(t)A_+(t)} , \\ A_-^*(t) &= -\frac{A_+(t)}{e^{2A_0(t)} - A_-(t)A_+(t)} , \\ e^{-A_0(t)-A_0^*(t)} &= 1 - A_-(t)A_+(t)e^{-2A_0(t)} , \end{aligned} \quad (20)$$

and hence

$$e^{A_0(t)-A_0^*(t)} = -\frac{A_-(t)}{A_+^*(t)} = -\frac{A_+(t)}{A_-^*(t)} . \quad (21)$$

Using (20) the following useful relationship follows

$$e^{-A_0(t)-A_0^*(t)} [1 - |A_-(t)|^2] = 1 . \quad (22)$$

It is not obvious that the explicit solutions Eq. (15) - Eq. (19) for $A_+(t)$, $A_-(t)$ and $A_0(t)$ satisfy the Eqs. (20). However, by using the fact that $A_+(t) = -e^{-i\Omega t}A_-(t)$ and various trigonometric relations, one can explicitly show that Eqs. (20) are fulfilled for all three cases $k^2 < 1$, $k^2 > 1$ and $k^2 = 1$.

With the solutions above it is now straightforward to calculate various expectation values and transition amplitudes. In this context it is useful to obtain the annihilation operator $a_H(t) \equiv a(t)$ in the Heisenberg picture ($a(t=0) \equiv a$), i.e.

$$a(t) = U(t)^\dagger a U(t) , \quad (23)$$

where

$$U(t) = U_0(t)U_I(t) , \quad (24)$$

and

$$U_0(t) = \exp[-i(\omega_a a^\dagger a + \omega_b b^\dagger b + E_0/2)t] . \quad (25)$$

Here $E_0 = \omega_a + \omega_b$ and $U_I(t)$ is given by Eq. (10). Straightforward calculations now gives

$$a(t) = e^{-A_0^*-i\omega_a t} [a - b^\dagger A_-^*(t)] , \quad (26)$$

from which $b(t)$ follows by the substitution $a \leftrightarrow b$. The creation operator a^\dagger follows from Eq. (26) by taking the Hermitian conjugate. When $k^2 = 0$ this solution for the operator $a(t)$ reduces to the wellknown result (see e.g. Ref.[14])

$$a(t) = a \cosh(gt) - b^\dagger \sinh(gt) . \quad (27)$$

The commutator $[a(t), a^\dagger(t)]$ is in general given by

$$[a(t), a^\dagger(t)] = e^{-A_0(t)-A_0^*(t)} [1 - |A_-(t)|^2] . \quad (28)$$

Due to Eq. (22) the quantum condition $[a(t), a^\dagger(t)] = 1$ is satisfied for all times, as it should be.

The Hamiltonian of the system is such that $a^\dagger(t)a(t) - b^\dagger(t)b(t)$ is a conserved quantity. We obtain

$$\begin{aligned} n_a(t) \equiv a^\dagger(t)a(t) = \\ a^\dagger a - A_-(t)K_- + A_+(t)e^{-2A_0(t)} (K_+ - 2A_-(t)K_0 + A_-^2(t)K_-) . \end{aligned} \quad (29)$$

Since $n_b(t) \equiv b^\dagger(t)b(t)$ can be obtained from Eq. (29) by means of the substitution $a \leftrightarrow b$ it follows immediately that $n_a(t) - n_b(t) = n_a(0) - n_b(0)$. The time-dependence of other combinations of annihilation and creation operators can be obtained in a similar manner.

4 Quantum Revivals

In this section we focus our attention on quantum revivals, i.e. when the initial state is reproduced by the time-evolution (for a reviews see e.g. Refs.[31]). The time-evolution operator Eq. (10) is written in a form that makes the evaluation of transition amplitudes $\langle f | U(t) | i \rangle$ straightforward. It is clear from the Eqs.(17) that exact quantum revivals will occur for Fock states only if $k^2 > 1$ and at revival times t_{rev} such that

$$gt_{rev}\sqrt{k^2 - 1} = n\pi , \quad (30)$$

where n is a positive integer. This is so since the corresponding transition probability is independent of Ω . The phase in the transition amplitudes due to the free time-evolution will not effect the transition probabilities, at least not for initial and final Fock-states. For coherent states we will, however, find it convenient to evaluate the transition probabilities in a basis in which case the free time-evolution is absent. For coherent states it then turns out that Eq. (30) is extended in such a way that only certain rational numbers of k^2 will

lead to revivals. Here we therefore see a remarkable difference between initial and final Fock states and coherent states respectively with regard to quantum revivals. We now treat these special cases in more detail.

4.1 Fock States

The two-mode initial state has now the form $|i\rangle = |r\rangle_a \otimes |s\rangle_b \equiv |r, s\rangle$. We also use the notation $\langle f | = {}_b\langle m | \otimes {}_a\langle n | \equiv \langle m, n |$. The transition amplitudes to be derived are $c_{mn}(t; r, s) \equiv \langle m, n | U_I(t) | r, s \rangle$. The probabilities to be calculated are then $p_{mn}(t; r, s) \equiv |c_{mn}(t; r, s)|^2$. We will suppress the initial state indices r and s if it is clear from the context what initial state we are considering. The corresponding amplitudes $c_{mn}(t)$ can be found in closed form by making use of the results from Section 3, i.e.

$$c_{mn}(t) = \delta_{m,s-r+n} \sqrt{r!s!m!n!} e^{A_0(t)(s+r+1)} \times \sum_{k=0}^{\min(r,s)} \frac{e^{-2kA_0(t)}}{(r-k)!(s-k)!} \frac{[A_-(t)]^k}{k!} \frac{[A_+(t)]^{n+k-r}}{(n+k-r)!} . \quad (31)$$

It follows from the actual expressions for $A_0(t)$, $A_+(t)$ and $A_-(t)$ that $|c_{mn}(t)|^2$ does not depend on Ω and therefore one obtain the revival times Eq. (30).

We now present more explicit results in a few simple cases. If the initial state is the vacuum state, i.e. $r = s = 0$, it follows that

$$p_{mn}(t) = \delta_{mn} e^{A_0(t)+A_0^*(t)} (|A_+(t)|^2)^n . \quad (32)$$

It can now be shown explicitly that this probability distribution is properly normalized, i.e. $\sum_{m,n=0}^{\infty} p_{mn}(t) = 1$ for all times. $p_{mn}(t)$ can be explicitly evaluated by making use of trigonometric identities. One can then derive the useful results

$$x(t) \equiv e^{-A_0(t)-A_0^*(t)} = \frac{\sinh^2(gt\sqrt{1-k^2}) + 1 - k^2}{1 - k^2} , \quad (33)$$

$$y(t) \equiv |A_+(t)|^2 = |A_-(t)|^2 = \frac{\sinh^2(gt\sqrt{1-k^2})}{\sinh^2(gt\sqrt{1-k^2}) + 1 - k^2} , \quad (34)$$

and

$$n_0(t) \equiv -A_-(t)A_+(t)e^{-2A_0(t)} = \frac{\sinh^2(gt\sqrt{1-k^2})}{1 - k^2} , \quad (35)$$

valid for all k^2 . The reason why we use the notation $n_0(t)$ is the fact that Eq. (35) is nothing else but the expectation value of the number operator $n_a(t)$, as given by Eq. (29) (or

$n_b(t)$), in the initial vacuum state. We notice that the last three equations are connected in the following way: $x(t)y(t) = n_0(t)$ and $x(t) = 1 + n_0(t)$.

The reduced density matrix for the a -modes (or the b -modes) is again given in terms of Eq. (32). As has been noticed before (see e.g. Refs.[5, 7, 8, 9, 10]) the reduced density matrices describe a system at finite temperature $T = 1/\beta$ such that $\exp(-\beta\omega) = y(t)$, where $\omega = \omega_a$ (or $\omega = \omega_b$ for the b -modes), i.e. if $k^2 < 1$ the temperature approaches infinity in the limit of large gt . This interpretation has, of course, a limited range of validity.

With $|i\rangle = |1, 1\rangle$, the corresponding probabilities are given by

$$p_{mn}(t) = \delta_{mn} \left(\frac{n^2}{x^2(t)} y^{n-1}(t) - \frac{2n}{x(t)} y^{n-1}(t) + y^{n+1}(t) \right) \frac{1}{x(t)} , \quad (36)$$

and again it follows that $p_{mn}(t)$ is properly normalized. Furthermore we have $\langle i|n_a(t)|i\rangle = 1 + 2n_0(t)$. The probabilities in Eq. (36) for $n = m = 1$ and $n = m = 3$ are shown in Fig. 1 for $k^2 = 1.5$ in which case quantum revivals are predicted. In Fig. 2 the same probabilities are shown, but now for the case $k^2 = 0.5$. These figures reflect the typical physical situation: For $k^2 < 1$ the probability has initially a peak structure and then it decays exponentially with time. Actually all probabilities $p_{mn}(t)$ will then tend to zero for sufficiently large times in such a way that their sum still is one, i.e. $\sum_{m,n=0}^{\infty} p_{mn}(t) = 1$. On the other hand, if $k^2 > 1$ the probability exhibit a totally different oscillatory behavior for all times with quantum revivals as predicted by Eq. (30). The reduced density matrices can be computed as above. For large gt and $k^2 < 1$ one finds that the reduced density matrices correspond to the same thermal distribution as for the initial vacuum state as discussed above.

Let us now assume that there is initially no b -quanta, that is $|i\rangle = |\psi\rangle_a \otimes |0\rangle_b$, where the initial a -mode state is a general pure state described by

$$|\psi\rangle_a = \sum_{s=0}^{\infty} \sqrt{\mathcal{P}_s} e^{i\phi_s} |s\rangle_a . \quad (37)$$

Here \mathcal{P}_s is the probability that the a -mode is in the Fock state $|s\rangle_a$ and ϕ_s is the corresponding phase. As above, the final states $U_0|r, s\rangle$ and $|r, s\rangle$ give the same result for the probability. The probability $p_{mn}(t) \equiv |\langle m, n| U_I(t) |\psi, 0\rangle|^2$ is given by

$$p_{mn}(t) = \mathcal{P}_{n-m} \frac{n!}{(n-m)! m!} \frac{y^m(t)}{x^{(n-m+1)}(t)} , \quad (38)$$

independent of the phase ϕ_n . Again one can analytically verify that $\sum_{m,n=0}^{\infty} p_{mn}(t) = 1$ for all times when $\sum_{n=0}^{\infty} \mathcal{P}_n = 1$ for all three cases $k^2 > 1$, $k^2 < 1$ and $k^2 = 1$. The expectation

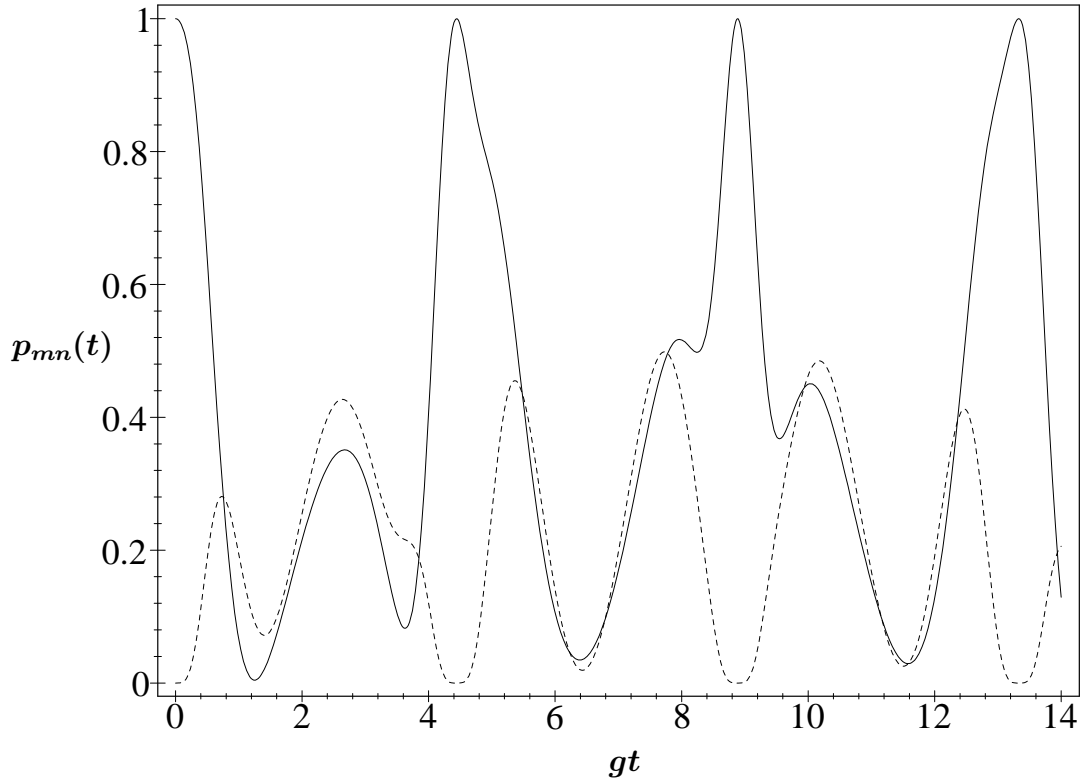


Figure 1: The probabilities $p_{11}(t; 1, 1)$ (solid curve) and $p_{33}(t; 1, 1)$ (dotted curve) when $k^2 = 1.5$ and with an initial vacuum state. The corresponding revival-times are integer multiples of $\pi\sqrt{2} \approx 4.44$.

values of the number operators for the a and b -modes are $\langle i | n_a(t) | i \rangle = \langle n_a \rangle + n_0(t)[\langle n_a \rangle + 1]$ and $\langle i | n_b(t) | i \rangle = n_0(t)[\langle n_a \rangle + 1]$ respectively. Here we have that $\langle n_a \rangle = \sum_{n=0}^{\infty} n \mathcal{P}_n$. If in particular the a -mode is Poisson distributed the probability $p_{12}(t)$ is shown in Fig. 3 for $k^2 = 0.5$ and $k^2 = 1.5$. When $k^2 > 1$ the probability oscillates between 0 and the maximum value of $p_{12}(t)$, i.e. $8|\alpha|^2 \exp(-|\alpha|^2)/27$ which is close to 0.104 for the parameters corresponding to Fig. 3. Furthermore, the case $k^2 = 1$ is very much like case $k^2 < 1$.

The reduced density matrices for the a - and b -modes are again diagonal with the matrix elements

$$p_m(b; t) = \sum_{n=0}^{\infty} p_{mn}(t) = \sum_{l=0}^{\infty} \mathcal{P}_l \frac{(l+m)!}{m! l!} \frac{y^m(t)}{x^{l+1}(t)} \quad , \quad (39)$$

for the b -modes and

$$p_n(a; t) = \sum_{m=0}^{\infty} p_{mn}(t) = \frac{1}{x^{n+1}(t)} \sum_{m=0}^n \mathcal{P}_{n-m} \binom{n}{m} n_0^m(t) \quad . \quad (40)$$

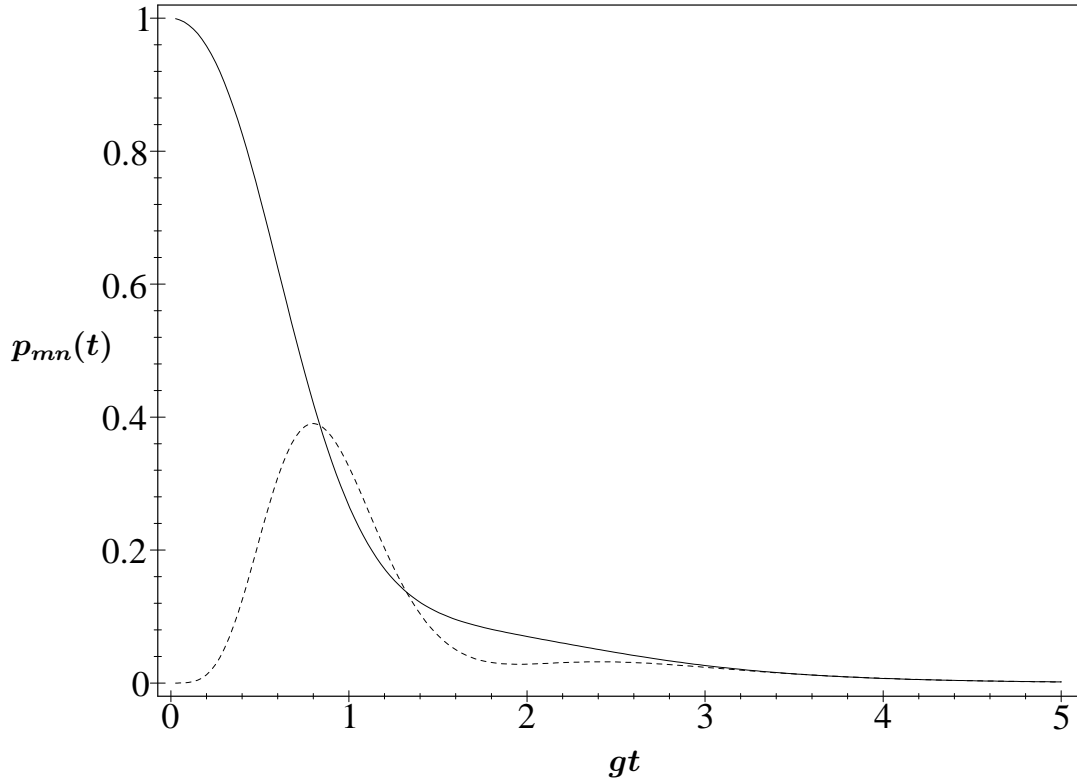


Figure 2: The probabilities $p_{11}(t; 1, 1)$ (solid curve) and $p_{33}(t; 1, 1)$ (dotted curve) when $k^2 = 0.5$ and with an initial vacuum state.

for the a -modes. For large gt and if $k^2 < 1$ one finds again that both modes are thermally distributed with the same distribution as in the case of an initial vacuum state.

4.2 Coherent State

We now consider initial and final coherent states. The coherent state transition amplitudes are somewhat general in the sense that all Fock-state amplitudes can be obtained from them in a standard manner (see e.g. Ref.[32]). If the final state is a coherent state, then the presence of $U_0(t)$ is important since $U_0(t) |\alpha\rangle_a \otimes |\beta\rangle_b = e^{-iE_0 t/2} |\alpha e^{-i\omega_a t}\rangle_a \otimes |\beta e^{-i\omega_b t}\rangle_b$. To exhibit quantum revivals we therefore find it convenient to use $U_0(t) |\alpha\rangle_a \otimes |\beta\rangle_b$ as a final state. Let us, in particular, consider the case when the system is initially in the coherent state $|i\rangle = |\alpha\rangle_a \otimes |\beta\rangle_b \equiv |\alpha, \beta\rangle$ and final state $\langle f| = b\langle z| \otimes_a \langle w| U_0^\dagger(t) \equiv \langle z, w| U_0^\dagger(t)$. The transition probability $p_{zw}(t) = |\langle z, w| U_I(t) |\alpha, \beta\rangle|^2$ is then given by

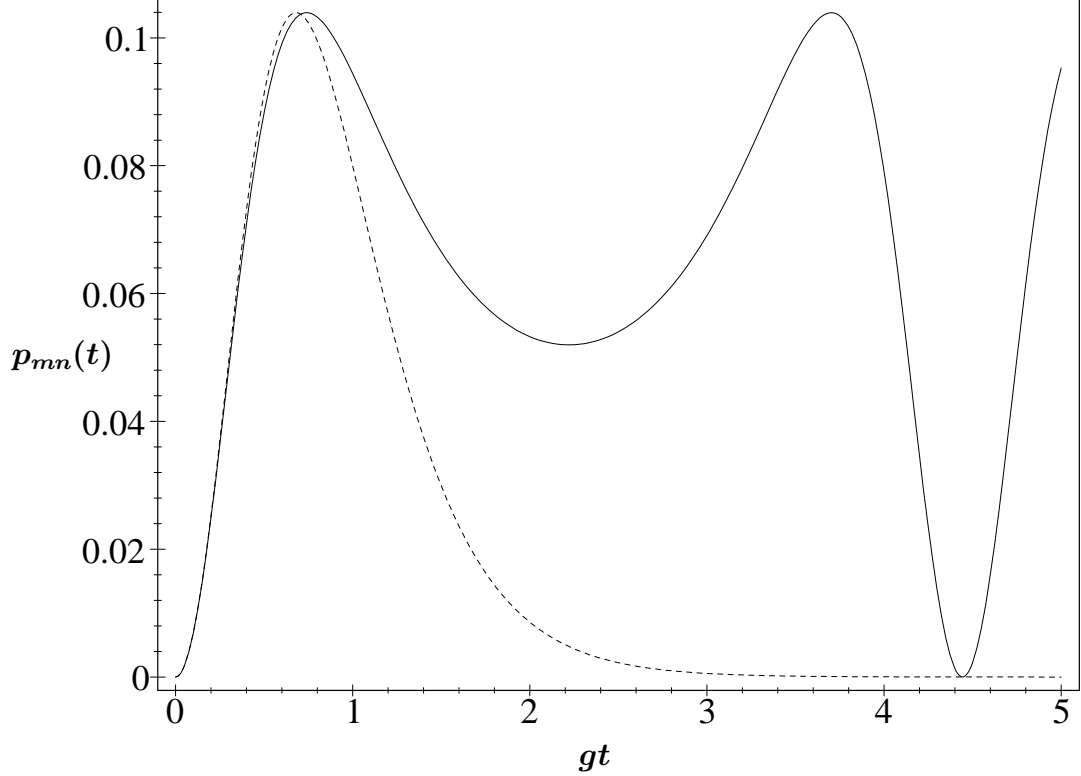


Figure 3: The probability $p_{mn}(t)$ in Eq. (38) when $n = 2$ and $m = 1$ for the two cases $k^2 = 1.5$ (solid curve) and $k^2 = 0.5$ (dotted curve) and when the a -photons initially are Poisson distributed $\mathcal{P}_n = |\alpha|^{2n} e^{-|\alpha|^2} / n!$ with amplitude $\alpha = 0.85$.

$$\begin{aligned}
p_{zw}(t) = & e^{-(|z|^2 + |w|^2 + |\alpha|^2 + |\beta|^2)} e^{A_0(t)} + A_0^*(t) \\
& \times |e^{A_+(t)} w^* z^*|^2 |e^{A_-(t)} \alpha \beta|^2 |e^{w^* \alpha e^{A_0(t)}}|^2 |e^{z^* \beta e^{A_0(t)}}|^2
\end{aligned} \quad (41)$$

Eq. (41) can be used as a generating function for the Fock state transition probabilities. The expectation value of the number operator for the a -mode is

$$\langle i | n_a(t) | i \rangle = \langle n_a \rangle + n_0(t)[\langle n_a \rangle + \langle n_b \rangle + 1] - 2\text{Re}[\alpha \beta A_-(t)](1 + n_0(t)) \quad , \quad (42)$$

and for the b -modes $\langle i | n_b(t) | i \rangle = \langle i | n_a(t) | i \rangle + \langle n_b \rangle - \langle n_a \rangle$. Here we have $\langle n_a \rangle = |\alpha|^2$ and $\langle n_b \rangle = |\beta|^2$. In contrast to the Fock case, this transition probability depends on the detuning frequency Ω . To obtain exact quantum revivals, the parameter k^2 can therefore not take an arbitrary value. To investigate the revival period of Eq. (41) it is convenient to rewrite the revival probability in the following form

$$\begin{aligned}
p_{\beta\alpha}(t) = & e^{-(|\alpha|^2 + |\beta|^2)[2 - e^{A_0(t)} - e^{A_0^*(t)}]} \\
& \times |e^{\alpha \beta [A_-(t) + A_+^*(t)]}|^2 |e^{A_0(t)} + A_0^*(t)|^2
\end{aligned} \quad . \quad (43)$$

By inspection of the actual expressions for $A_+(t)$ and $A_-(t)$ in Eq. (17) we see that the second factor in Eq. (43) is periodic when

$$k^2 = \frac{1}{1 - (p/n)^2} , \quad (44)$$

where n and p are integers satisfying $n > p$, i.e. k^2 has to be a rational number in order to obtain exact quantum revivals. From the first factor Eq. (43) we also see that $A_0(t)$ has to be periodic in order to observe revivals. Thus, we have further restrictions on the integers n and p : if n is even, then p must also be even. If n is odd, then p must also be odd. The revival time corresponding to Eq. (44) is then

$$gt_{rev} = \pi \sqrt{n^2 - p^2} . \quad (45)$$

The solid curve in Fig. 4 shows the probability $p_{\beta\alpha}(t)$ when $k^2 = 9/5$, i.e. when k^2 satisfies Eq. (44) ($\alpha = \beta = 1$). The revival times are then integer multiples of $gt_{rev} = \pi\sqrt{20} \approx 14.05$.

When the parameter k^2 does not satisfy Eq. (44) the time-dependence of $p_{\beta\alpha}(t)$ is much more complicated. As long as $|\alpha| \neq 0$ and $|\beta| \neq 0$ the probability in Eq. (43) will then never reach unity. Hence, there are no revivals. But as we can see from Fig. 4 the probability $p_{\beta\alpha}(t)$ nevertheless exhibits some peaks at e.g. $gt \approx 22$ and $gt \approx 41$ (dotted curve). These times correspond to the condition $2 - \exp[A_0(t)] - \exp[A_0^*(t)] \approx 0$, due to the first factor in Eq. (43). If this condition is not satisfied $p_{\beta\alpha}(t)$ will be exponentially suppressed when α and β are large, i.e. when the photon number is large.

5 Non-Classical Behavior

Our two-mode system exhibits quantum correlations. These correlations can be described by various correlations functions. We find it convenient to consider the following well-defined second-order correlations function:

$$f(t) \equiv \sqrt{\langle (a^\dagger)^2 a^2 \rangle} \sqrt{\langle (b^\dagger)^2 b^2 \rangle} - \langle a^\dagger a b^\dagger b \rangle , \quad (46)$$

where e.g.

$$\langle a^\dagger a b^\dagger b \rangle \equiv \langle i | U^\dagger(t) a^\dagger a b^\dagger b U(t) | i \rangle . \quad (47)$$

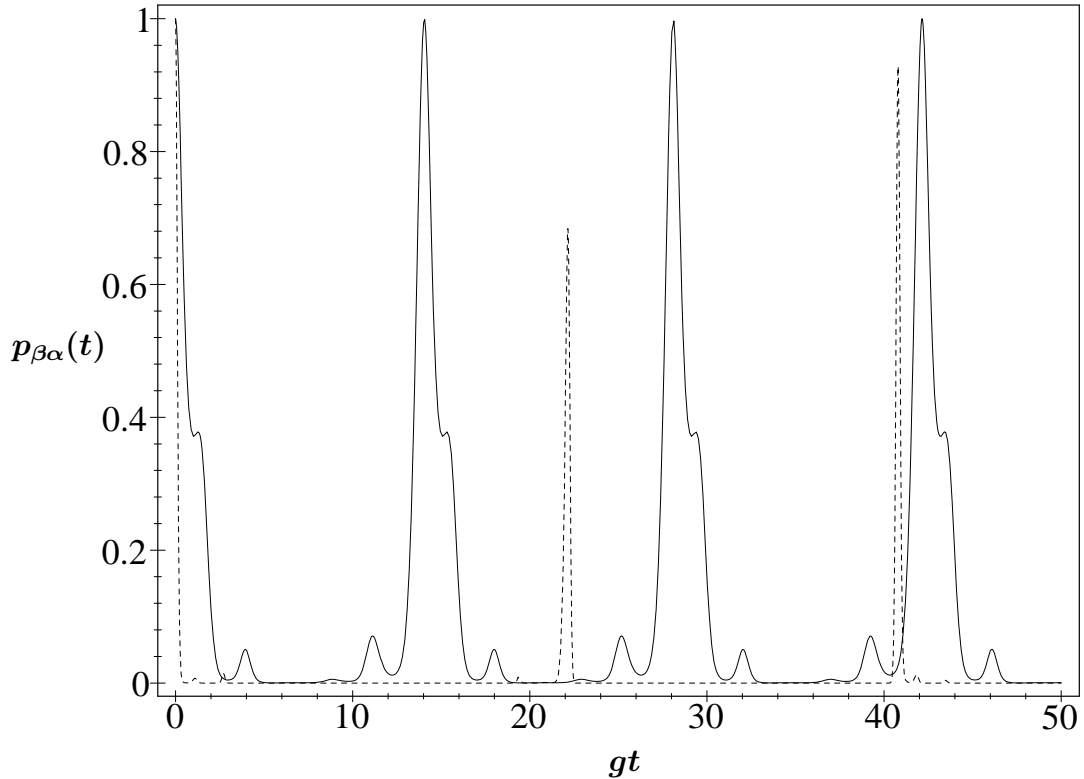


Figure 4: The solid curve shows the probability $p_{\beta\alpha}(t)$ when $k^2 = 9/5$ and $\alpha = \beta = 1$. The dotted curve shows $p_{\beta\alpha}(t)$ when $k^2 = \pi$ and $\alpha = \beta = 5$. The revival times corresponding to the solid curve are integer multiples of $gt_{rev} = \pi\sqrt{20} \approx 14.05$.

Since the expectation-values in Eq. (46) are normal-ordered we can always write these moments in terms of a Glauber-Sudarshan P representation, e.g.

$$\langle a^\dagger a b^\dagger b \rangle = \int d^2\alpha \int d^2\beta |\alpha|^2 |\beta|^2 P(\alpha, \beta; t) . \quad (48)$$

If $P(\alpha, \beta; t)$ is real and positive, then the moments in Eq. (46) are defining inner products. Hence, the Cauchy-Schwarz inequality implies the $f(t) \geq 0$. States described by such a function admit a classical interpretation where the complex field amplitudes α and β may be treated as stochastic random variables with the joint probability distribution $P(\alpha, \beta; t)$. If, however, $f(t) < 0$ then $P(\alpha, \beta; t)$ is not real and positive everywhere. In such a situation the correlations cannot be described classically since $P(\alpha, \beta; t)$ cannot be interpreted as a classical probability distribution. Hence, the sign of $f(t)$ reflects the classical or quantum nature of the correlations between the modes.

Another convenient way to characterize a non-classical state for single modes is the Mandel quality factor Q_a defined by [15]

$$Q_a(t) = \frac{\langle (\Delta n_a(t))^2 \rangle - \langle n_a(t) \rangle}{\langle n_a(t) \rangle} , \quad (49)$$

where $n_a(t) \equiv a^\dagger(t)a(t)$ and $(\Delta\mathcal{O}(t))^2 \equiv \text{Var}[\mathcal{O}(t)] \equiv \langle \mathcal{O}^2(t) \rangle - \langle \mathcal{O}(t) \rangle^2$ for an observable \mathcal{O} . The quality factor is constructed in such a way that $Q_a = 0$ when the statistics describing the isolated a -quanta is Poissonian. If the Q_a factor is negative the state is quantum mechanical, without any classical analog. In this case the statistics is sub-Poissonian. The smallest value -1 is obtained for a Fock state. On the other hand, when Q_a is positive the statistics is super-Poissonian and the isolated a -mode can be described in classical terms. A corresponding formula as Eq. (49) holds for the b -quanta.

5.1 Fock States

Let us now consider the situation with initial Fock states $|r\rangle_a \otimes |s\rangle_b \equiv |r, s\rangle$. The Mandel factor in this case is given by

$$Q_a(t) = \frac{n_0(t) \ 2rs + n_0^2(t) \ [2rs + r + s + 1] - r}{r + n_0(t) \ [r + s + 1]} , \quad (50)$$

where $n_0(t)$ is as in Eq. (35). If $r = 0$ then $Q_a(0) = 0$, independent of s , see e.g. Fig. 5 (dotted curve). On the other hand, if $r \neq 0$ then $Q_a(0) = -1$, also independent of s , see e.g Fig. 5 (thin solid curve). The physics when $t > 0$ depends strongly on the value of k^2 . If $k^2 < 1$ the Mandel factor increase exponentially with time, which leads to super-Poissonian statistics of the a -quanta. If, on the other hand, $k^2 > 1$ then the $Q_a(t)$ -function will have an oscillatory behavior. The maximum value of $Q_a(t)$, when $r \neq 0$ and $s = 0$, is $Q_a^{max} = [1 + 1/r - (k^2 - 1)^2]/[(k^2 - 1)^2 + (k^2 - 1)(1 + 1/r)]$. If $r = 0$ and $s \neq 0$ then $Q_a^{max} = 1/(k^2 - 1)$. The minimum value of $Q_a(t)$ is 0 or -1 , depending on the value of r as discussed above (c.f. Fig. 5).

The $f(t)$ -function when the system is initially in the Fock state $|r, s\rangle$ is given by

$$\begin{aligned} f(t) = & x^2(t) \ \sqrt{r(r-1) + 4r(s+1)y(t) + (s+1)(s+2)y^2(t)} \\ & \times \sqrt{s(s-1) + 4s(r+1)y(t) + (r+1)(r+2)y^2(t)} \\ & - x^2(t) \ [rs + (r+1)(s+1)y^2(t) \\ & + (rs + r(r+1) + s(s+1) + (r+1)(s+1)) y(t)] , \end{aligned} \quad (51)$$

where $x(t)$ is given by Eq. (33) and $y(t) = 1 - 1/x(t)$ as in Eq. (34). Notice that $f(t)$ is symmetric with respect to exchange of r and s as it should.

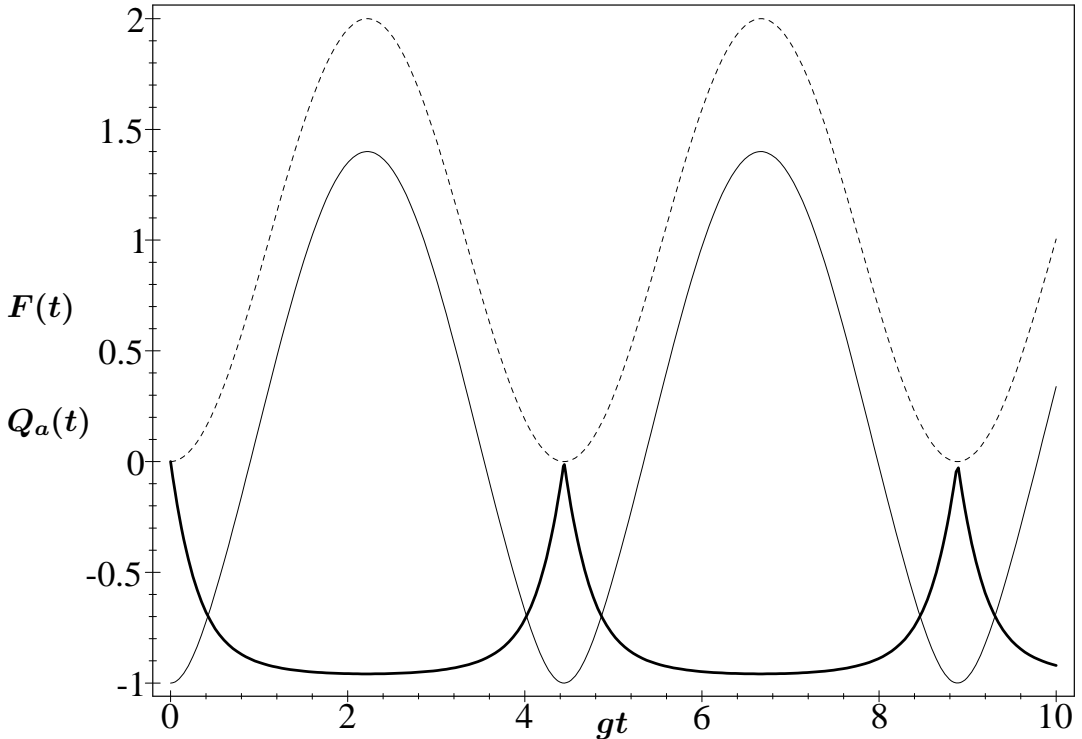


Figure 5: The Mandel factor $Q_a(t)$ when the system is in the Fock state $|r\rangle_a \otimes |s\rangle_b$ and when $k^2 = 1.5$. The thin solid curve correspond to $r = 1, s = 0$ and the dotted curve correspond to $r = 0, s = 1$. The thick solid curve shows the corresponding $F(t)$ -function.

Let us now, for reasons of convenience, consider the correlation function $F(t) \equiv f(t)/\sqrt{\langle n_a(t) \rangle \langle n_b(t) \rangle}$ instead of $f(t)$ itself. Fig. 5 shows $F(t)$ as well as the corresponding quality factors for $k^2 = 1.5$ and $r = 1, s = 0$ or $r = 0, s = 1$. The $F(t)$ -function in this figure is negative for all times, except at the revival times where it is zero, and the two-mode down-converted light therefore exhibits quantum mechanical correlations in this case. Since the Fock state is a typical quantum mechanical state this result is as expected. Nevertheless, the quality factor oscillates between 0 and 2 (dotted curve) indicating that the statistics of the isolated a -system is super-Poissonian. It is, however, possible to make $F(t)$ positive in spite of the fact that the Fock state is a typical quantum mechanical state. This can be done by choosing $r \gg s \neq 0$ or vice versa (e.g. $r = 50$ and $s = 10$ as in Fig. 6 (thin solid curve)). If $r = s$ then $F(t) = -1$ for all possible values of k^2 , c.f. the thick line in Fig. 6. If $s = 0$ then $F(t) \leq 0$ also for all k^2 . Fig. 7 shows the typical behavior when $k^2 < 1$. As we can see, $F(t)$ approaches -1 for sufficiently large times. Furthermore, the thin dotted curve in Fig. 7 is negative for all times, but the

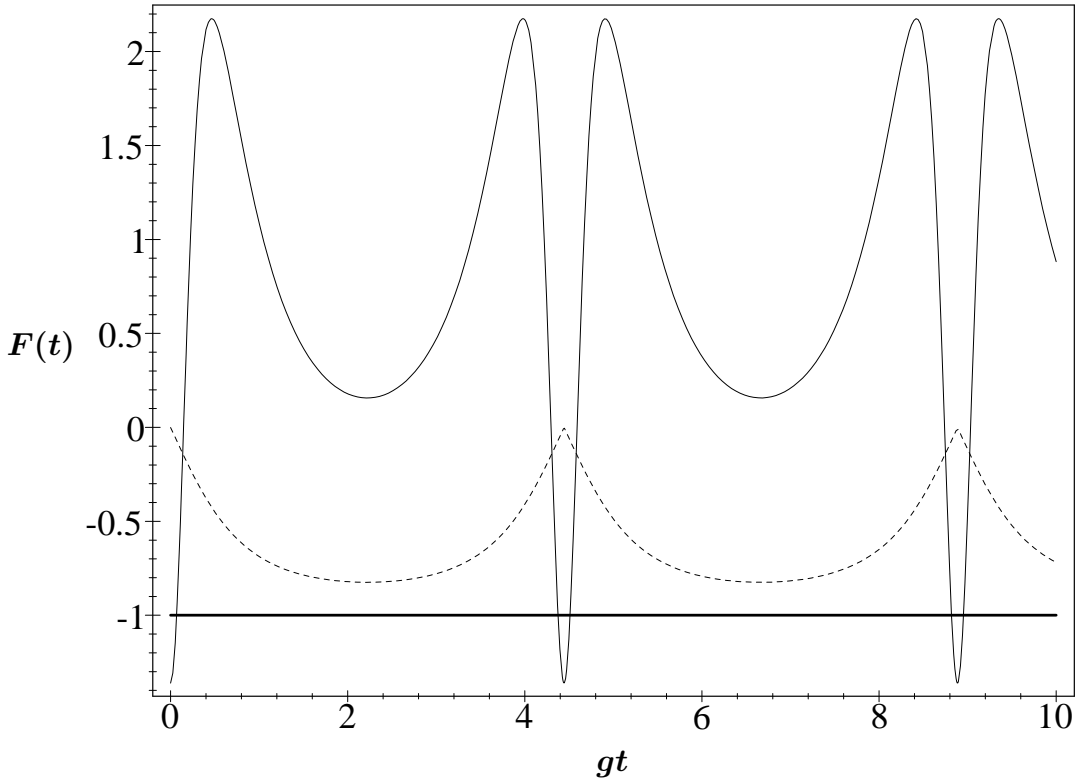


Figure 6: The normalized function $F(t) \equiv f(t)/\sqrt{n_a(t)n_b(t)}$ when $k^2 = 1.5$. The thin solid curve shows $F(t)$ when the system is initially a Fock state $|r\rangle_a \otimes |s\rangle_b$ with $r = 50, s = 10$ and the dotted curve when $r = 50, s = 0$. The thick solid curve corresponds to arbitrary $r = s$.

thin solid curve has a positive peak at small times ($0.1 \lesssim gt \lesssim 1.3$). In this short period of time the correlation between the a - and b -mode can be described in classical terms. For all other times, when $F(t)$ is negative, the down-converted quanta exhibits quantum mechanical correlations. Furthermore, the corresponding Mandel factor starts at -1 or 0 (depending on the value of r) and increase exponentially with time.

As mentioned earlier, in the case $k^2 < 1$, the isolated a - or b -mode describes a system with a temperature that approaches infinity in the large gt limit. It is therefore expected that the statistics become super-Poissonian in this limit.

5.2 Coherent States

Since the quantum mechanical state that corresponds to a classical description is the coherent state, we expect classical-like behavior when considering initial and final coherent states. Fig. 8 shows the function $F(t)$ for the initial coherent state $|\alpha\rangle_a \otimes |\beta\rangle_b \equiv |\alpha, \beta\rangle$

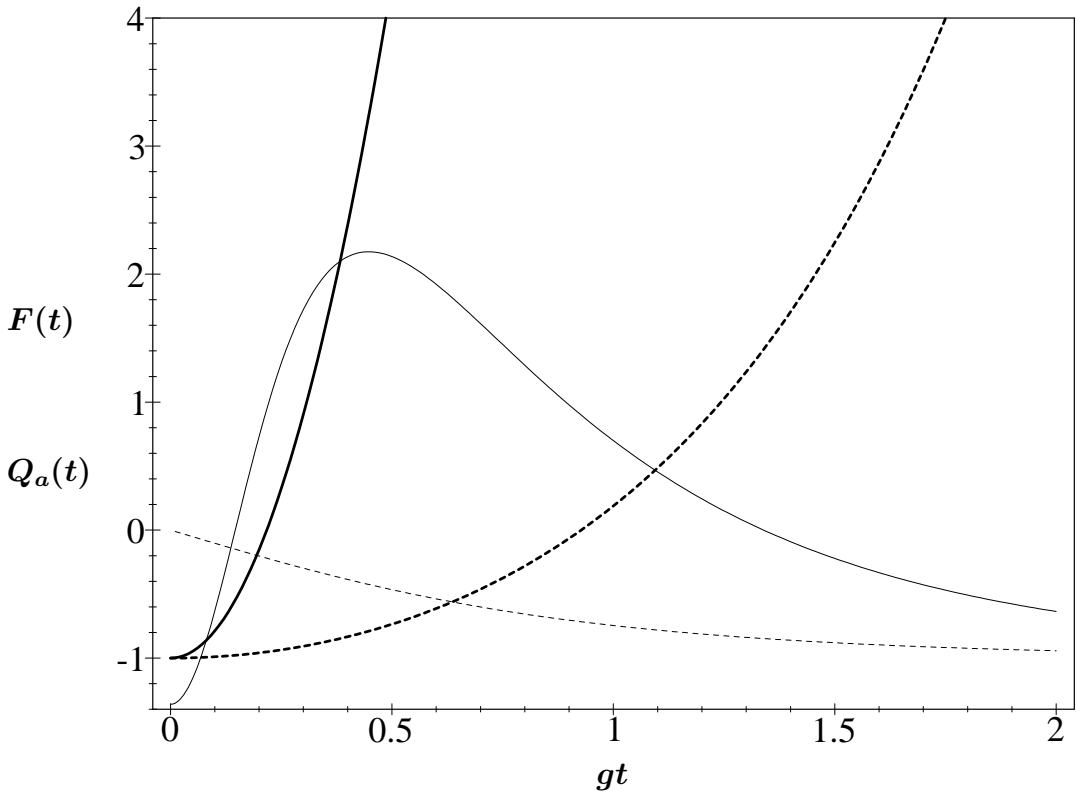


Figure 7: All curves correspond to $k^2 = 0.5$. The thin solid curve shows $F(t)$ when the two-mode system is initially in the Fock state $|r\rangle_a \otimes |s\rangle_b \equiv |r, s\rangle$ with $r = 50$, $s = 10$. The thick solid curve is the corresponding $Q_a(t)$ -factor. The thin dotted curve shows $F(t)$ in the case $r = 50$, $s = 0$ and the thick dotted curve is the corresponding $Q_a(t)$ -factor.

when $k^2 = 1.5$. For reasons of comparison we have chosen the expectation-value of the photon number to be the same as in the Fock case in Fig. 6. We see that for coherent states $F(t)$ is mostly negative (solid curve in Fig. 8) while for Fock states $F(t)$ is mostly positive (solid curve in Fig. 6). This illustrates the surprising fact that the correlation between the modes can be even more quantum mechanical for coherent states as compared to initial Fock states with the same average number of photons.

6 Squeezing and Detuning

In this section we will consider the influence of detuning on squeezing. The squeezing will be defined with respect to the phase-dependent quadrature amplitude $X_\theta(t)$ (see e.g.

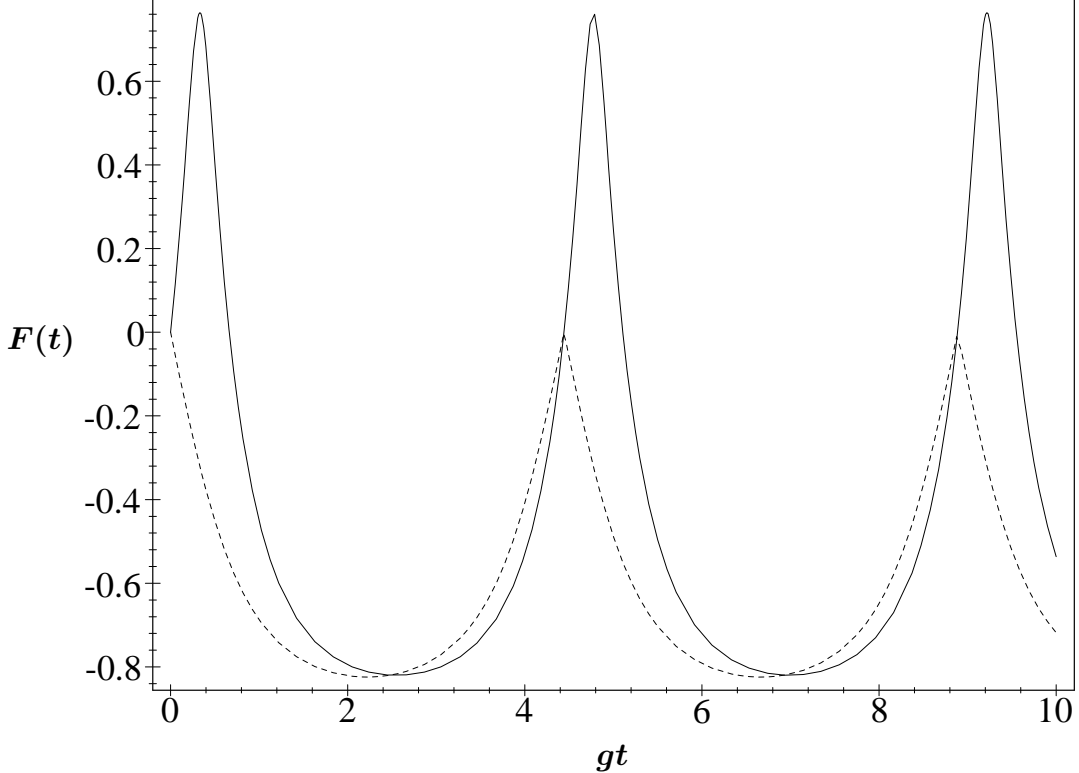


Figure 8: The correlation function $F(t) \equiv f(t)/\sqrt{\langle n_a(t) \rangle \langle n_b(t) \rangle}$ when $k^2 = 1.5$. The solid curve shows $F(t)$ when the system is initially a coherent state $|\alpha\rangle_a \otimes |\beta\rangle_b$ with $\alpha = \sqrt{50}$, $\beta = \sqrt{10}$ and the dotted curve when $\alpha = \sqrt{50}$, $\beta = 0$.

Ref.[14]):

$$X_\theta(t) = \frac{1}{\sqrt{2}} \{ a(t)e^{i\theta t} + b(t)e^{-i\theta t} + h.c. \} . \quad (52)$$

A number of schemes to make quadrature phase measurements have been discussed in the literature (see e.g. Ref.[14]). These schemes involve homodyning the signal field with a reference signal known as the local oscillator. In this case θ is the phase of the local oscillator. The variables $X_0(t)$ and $X_{\pi/2}(t)$ are canonical, i.e. they obey the commutation relation

$$[X_0, X_{\pi/2}] = -2i . \quad (53)$$

The corresponding uncertainty product therefore is

$$\Delta X_0 \Delta X_{\pi/2} \geq 1 . \quad (54)$$

We now consider squeezing in terms of the observable $X_\theta(t)$ for initial Fock states or coherent states.

6.1 The Fock State

If the system initially is in the Fock state $|r, s\rangle$ the variance in $X_\theta(t)$ is expressed by

$$Var[X_\theta(t)] = |T_\theta(t)|^2 (r + s + 1) , \quad (55)$$

where

$$\begin{aligned} |T_\theta(t)|^2 &\equiv |e^{-A_0^*(t) + i\theta} - A_-(t) e^{-A_0(t) - i\theta}|^2 \\ &= x(t) [1 + y(t) - 2(\cos(\Omega t - 2\theta)G(t) + \sin(\Omega t - 2\theta)H(t))] . \end{aligned} \quad (56)$$

Here we have defined the functions

$$G(t) = \begin{cases} \sqrt{k^2 - 1} \frac{\tan(gt\sqrt{k^2 - 1}) [1 - \tanh^2 \delta]}{\tan^2(gt\sqrt{k^2 - 1}) + \tanh^2 \delta} , & \text{if } k^2 \geq 1 \\ \sqrt{1 - k^2} \frac{\tanh(gt\sqrt{1 - k^2}) [1 + \tan^2 \gamma]}{1 + \tanh^2(gt\sqrt{1 - k^2}) \tan^2 \gamma} , & \text{if } k^2 \leq 1 \end{cases} \quad (57)$$

and

$$H(t) = \begin{cases} \sqrt{k^2 - 1} [\coth \delta - \frac{\tanh \delta [1 + \tan^2(gt\sqrt{k^2 - 1})]}{\tan^2(gt\sqrt{k^2 - 1}) + \tanh^2 \delta}] , & \text{if } k^2 \geq 1 \\ \sqrt{1 - k^2} [\tan \gamma - \frac{\tan \gamma [1 - \tanh^2(gt\sqrt{1 - k^2})]}{1 + \tanh^2(gt\sqrt{1 - k^2}) \tan^2 \gamma}] , & \text{if } k^2 \leq 1 \end{cases} . \quad (58)$$

$x(t)$ and $y(t)$ are given by Eq. (33) and Eq. (34), respectively. The expressions for $\tan \gamma$ and $\coth \delta$ are, furthermore, given by Eq. (16) and Eq. (18). The special case when $k^2 = 0$ the variance in Eq. (55) reduces to

$$Var[X_0(t)] = e^{-2gt}(r + s + 1) , \quad (59)$$

and

$$Var[X_{\pi/2}(t)] = e^{2gt}(r + s + 1) , \quad (60)$$

in agreement with well known results (see e.g. [14]). We immediately see that this is a minimum-uncertainty state when $r = s = 0$. Therefore, changing the phase of the local oscillator, θ , by $\pi/2$ enables one to move from enhanced to squeezed quadrature phase fluctuations.

By inspection of the actual expressions for $A_+(t)$ and $A_-(t)$ in Eq. (17) we see that Eq. (56) is periodic when k^2 satisfies Eq. (44). The corresponding revival time is therefore

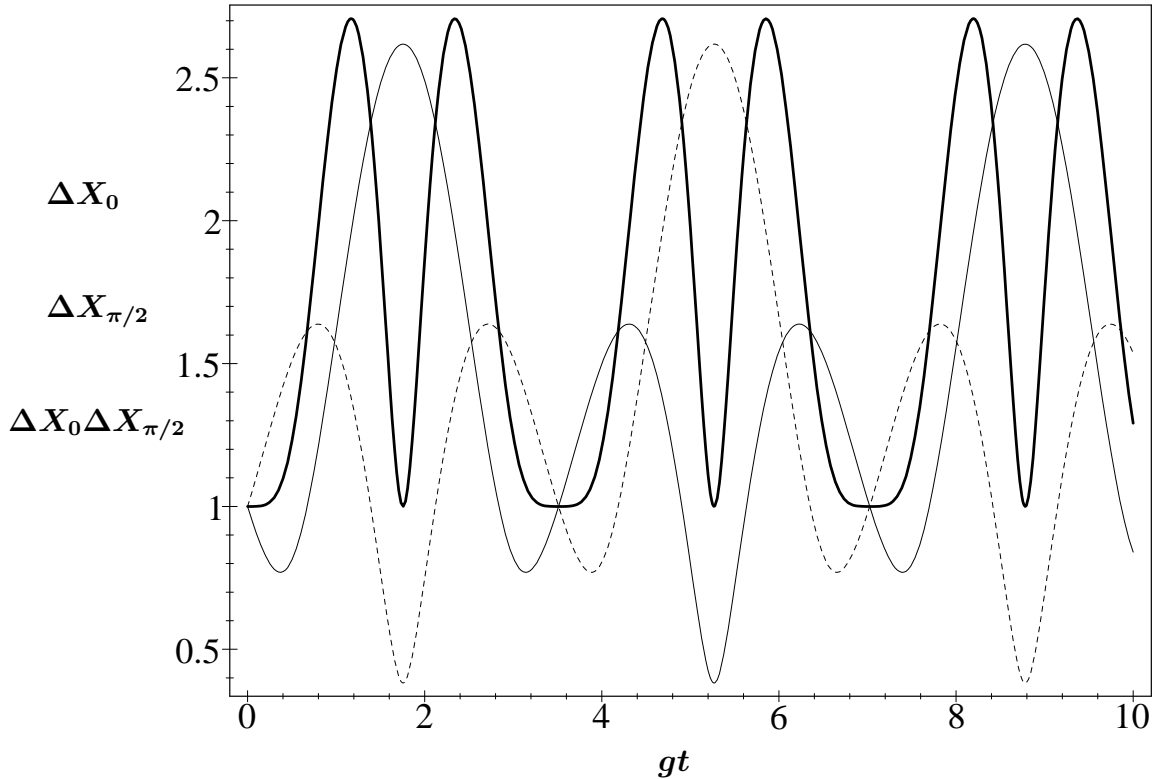


Figure 9: The thin solid curve shows $\Delta X_0(t)$, the dotted curve shows $\Delta X_{\pi/2}(t)$. The thick solid curve is the corresponding uncertainty product. All curves correspond to the vacuum case and $k^2 = 9/5$.

again given by Eq. (45). Fig. 9 shows the uncertainties $\Delta X_0(t) \equiv \sqrt{\text{Var}[X_0(t)]}$ (thin solid curve) and $\Delta X_{\pi/2}(t) \equiv \sqrt{\text{Var}[X_{\pi/2}(t)]}$ (dotted curve) when the system is initially in vacuum for $k^2 = 9/5$. These curves oscillate with the period $gt_{\text{rev}} = \pi\sqrt{5} \approx 7.02$, where we can choose $p = 2$ and $n = 3$. However, the period of the uncertainty product is just half the period of the individual uncertainties, i.e. uncertainty product oscillate with period $gt = \pi\sqrt{5}/2 \approx 3.51$. This is due to the fact that $\text{Var}[X_0(t + t_{\text{rev}}/2)] = \text{Var}[X_{\pi/2}(t)]$, i.e. the curve $\text{Var}[X_{\pi/2}(t)]$ is just shifted $t_{\text{rev}}/2$ relative to $\text{Var}[X_0(t)]$.

Due to revivals the uncertainty product is one at the revival times. The uncertainties $\Delta X_0(t)$ and $\Delta X_{\pi/2}(t)$ are then equal and there is no squeezing. We now observe that we can write $\Delta X_0^2(t) = c(t) + d(t)$ and $\Delta X_{\pi/2}^2(t) = c(t) - d(t)$, i.e. the uncertainty product is $\Delta X_0^2(t)\Delta X_{\pi/2}^2(t) = c^2(t) - d^2(t)$, where the functions $c(t)$ and $d(t)$ can be obtained from Eq. (56). From this observation we infer that extremal values of $\Delta X_0(t)$ and $\Delta X_{\pi/2}(t)$ are associated with extremal values of the uncertainty product. This fact is also clearly illustrated in Fig. 9.

Let us now study the case $k^2 < 1$. Fig. 10 shows a logarithmic plot of the uncertainties

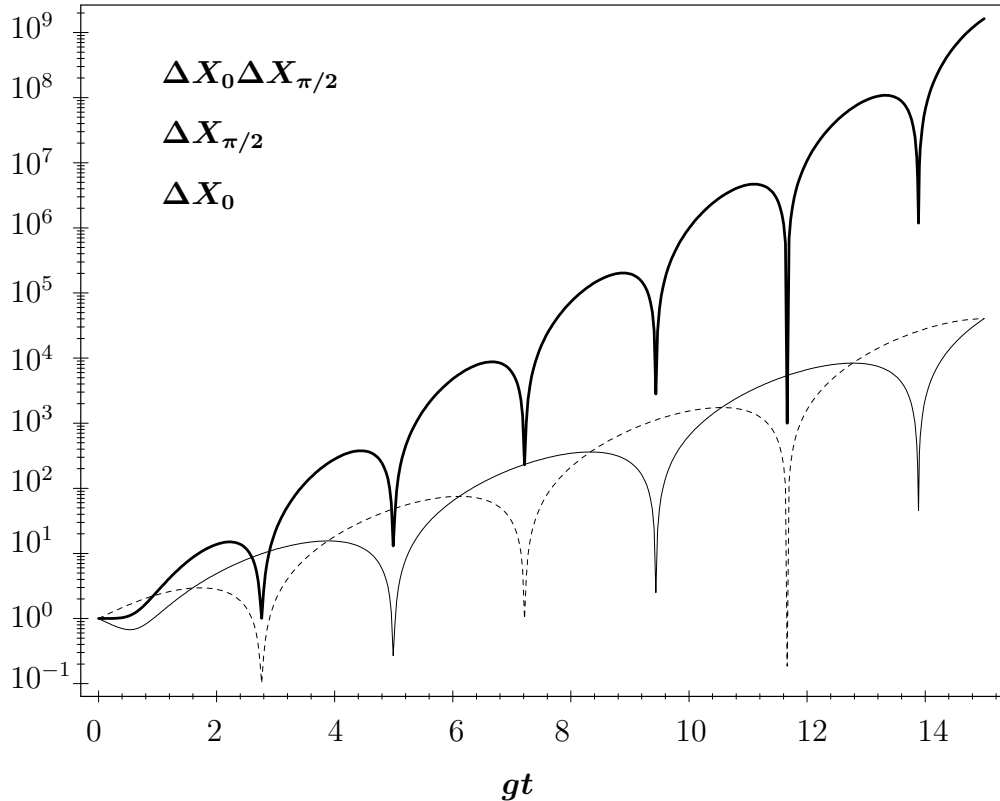


Figure 10: The thin solid curve shows $\Delta X_0(t)$, the dotted curve shows $\Delta X_{\pi/2}(t)$. The thick solid curve is the corresponding uncertainty product. All curves correspond to the vacuum case and $k^2 = 0.5$.

$\Delta X_0(t)$ and $\Delta X_{\pi/2}(t)$ and the corresponding uncertainty product when the system is initially in the vacuum state and $k^2 = 0.5$. As we can see, the uncertainties increase essentially at an exponentially rate as a function of time. However, the curves also exhibit an oscillatory behavior with various local minima. These minima actually occur when the time-derivative of Eq. (56) is equal to zero. When $gt\sqrt{1-k^2} \ll 1$ the derivative of this equation is complicated and the various minima must be determined numerically. When $gt\sqrt{1-k^2} \gg 1$ the periodicity for large gt is determined by the the cosine- and sine-functions in Eq. (56), i.e. the local minima of $\Delta X_0(t)$ and $\Delta X_{\pi/2}(t)$ have a period $gt = \pi/k$. The period of the uncertainty product is half of this period, as discussed above.

6.2 The Coherent State

The coherent case, when the a -and b -mode are initially in the coherent state $|\alpha, \beta\rangle$,

the variance of $X_\theta(t)$ is given by

$$Var[X_\theta(t)] = |T_\theta(t)|^2 , \quad (61)$$

where again $|T_\theta(t)|^2$ is given by Eq. (56). The most striking feature of Eq. (61) is the fact that it is independent of the initial values of α and β . Moreover, the only difference between the Fock variance in Eq. (55) and the coherent variance in Eq. (61) is the factor $r + s + 1$. The coherent state variances are therefore equal to the vacuum state variances.

7 Signal-to-Noise Ratio

We define the signal-to-noise ratio $\rho_a(t)$ for the a -mode by

$$\rho_a(t) = \frac{\langle n_a(t) \rangle}{\sqrt{\langle Var[n_a(t)] \rangle}} , \quad (62)$$

where $n_a(t) \equiv a^\dagger(t)a(t)$, see Eq. (29). A similar definition for the b -mode holds. To get a good signal we want such ratios to be as large as possible. Let us suppose the system is initially in the Fock state $|r, s\rangle$. The ratio $\rho_a(t)$ is then given by

$$\rho_a(t) = \frac{r + n_0(t)(r + s + 1)}{\sqrt{n_0(t) + n_0^2(t)}} \frac{1}{\sqrt{2rs + r + s + 1}} , \quad (63)$$

where $n_0(t)$ is given by Eq. (35). The small and large time limits of $\rho_a(t)$ are

$$\rho_a(t) = \begin{cases} \frac{r + s + 1}{\sqrt{2rs + r + s + 1}} & , \text{ if } t \rightarrow \infty , k^2 < 1 , \\ \frac{r + (gt)^2(r + s + 1)}{gt\sqrt{2rs + r + s + 1}} & , \text{ if } t \rightarrow 0 , \text{ for all } k^2 . \end{cases} \quad (64)$$

If $r = 0$ we then have a well-defined limit for small times, i.e. $\rho_a(0) = 0$ (see e.g. Fig. 11 (thick curves)). On the other hand, if $r \neq 0$ then $\rho_a(0) = \infty$ (see e.g. Fig. 11 (thin curves)). This is due to the fact that a Fock state has no variance. The behavior of $\rho_a(t)$ at $t > 0$ depends strongly on k^2 . If $k^2 < 1$ the signal-to-noise ratio approaches the value as given in Eq. (64). If, on the other hand, $k^2 > 1$ the ratio $\rho_a(t)$ will oscillate. The period of $\rho_a(t)$ is determined by Eq. (35), i.e. the revival time is

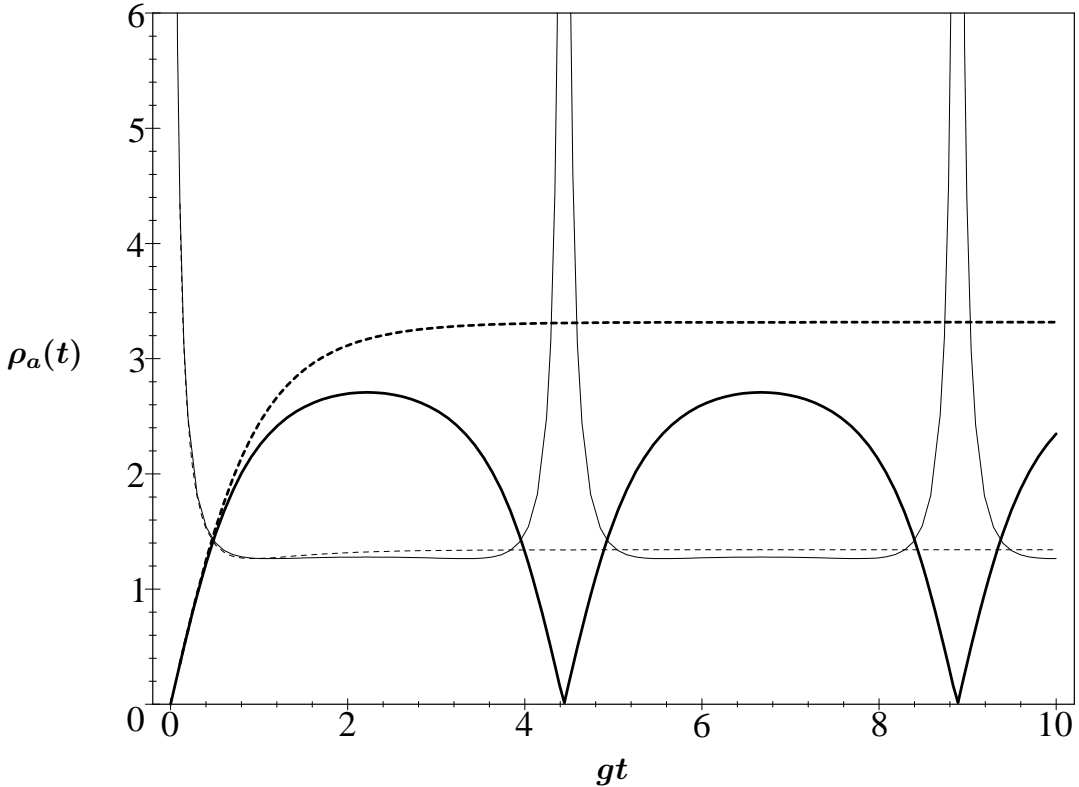


Figure 11: The thin curves show $\rho_a(t)$ when $r = 1, s = 1$. The thin solid curve corresponds to $k^2 = 1.5$ and the thin dotted one corresponds to $k^2 = 0.5$. The thick curves show $\rho_a(t)$ when $r = 0, s = 10$. The thick solid curve corresponds to $k^2 = 1.5$ and the thick dotted one corresponds to $k^2 = 0.5$. The revival time is $gt_{rev} = \sqrt{2}\pi \approx 4.44$.

$$gt_{rev}\sqrt{k^2 - 1} = n\pi , \quad (65)$$

where n is a positive integer. The value of $\rho_a(t)$ at the revival time is 0 or ∞ , depending on the value of r as discussed above (see e.g. Fig. 11). Therefore, we can achieve an infinite signal-to-noise ratio at the revival times by choosing $r \neq 0$.

Another interesting feature of the signal-to-noise ratio $\rho_a(t)$ is that it can be approximatively constant between revival times, which also is illustrated in Fig. 11. This is to be compared with the oscillatory behavior of e.g. $p_{11}(t)$ ($p_{11}(t)$ in Fig. 1 is oscillating fast for times where $\rho_a(t)$ is approximately constant).

Let us now study the extrema of the signal-to-noise ratio, i.e. when the time derivative of Eq. (63) is zero. $\rho_a(t)$ has always an extremum when

$$gt\sqrt{k^2 - 1} = n\pi/2 , \quad (66)$$

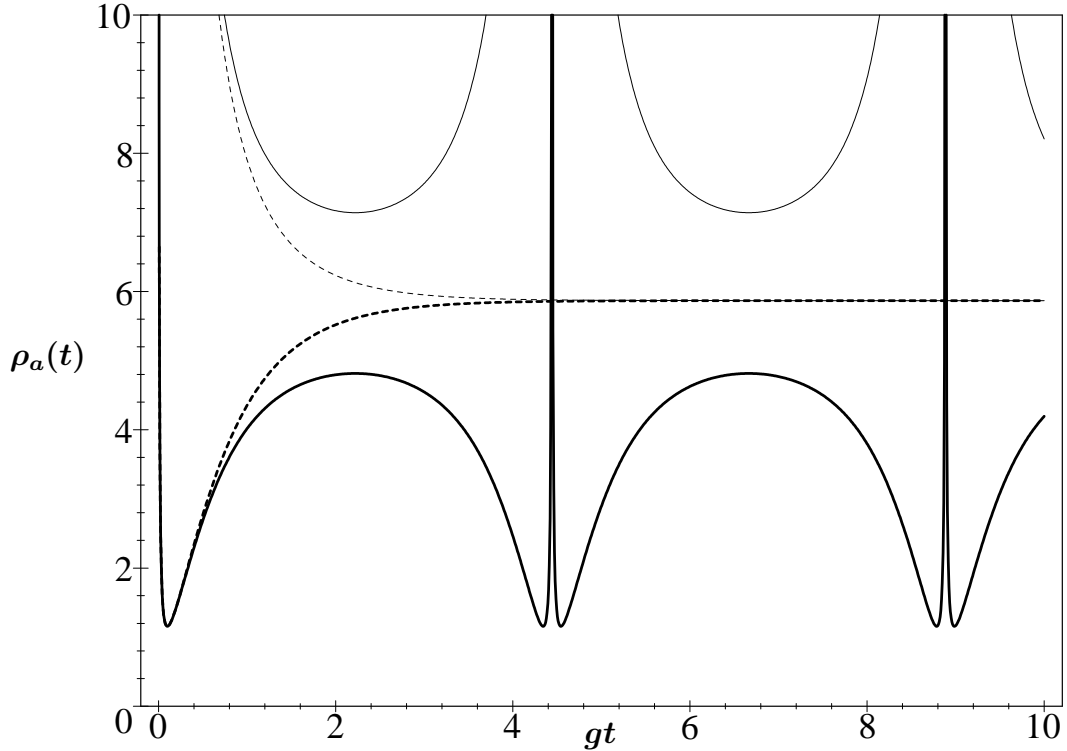


Figure 12: The thin curves show $\rho_a(t)$ when $r = 100, s = 1$. The thin solid curve corresponds to $k^2 = 1.5$ with the global minimal value $\rho_a^{extr} = 152/\sqrt{452} \approx 7.15$. The thin dotted one corresponds to $k^2 = 0.5$. The thick curves correspond to the case $r = 1, s = 100$. The thick solid curve show $\rho_a(t)$ when $k^2 = 1.5$ with the local maximal value $\rho_a^{extr} = 205/(2\sqrt{452}) \approx 4.82$. The thick dotted one corresponds to $k^2 = 0.5$. Both dotted curves approach the value $\rho_a = 102/\sqrt{302} \approx 5.87$.

where n is an odd integer. The value $\rho_a(t)$ at these particular times is

$$\rho_a^{extr} = \frac{rk^2 + s + 1}{\sqrt{k^2(2rs + r + s + 1)}} . \quad (67)$$

If, in addition, r, s and $k^2 (> 1)$ satisfy the inequality

$$0 < \frac{r}{s - r + 1} < \frac{1}{k^2 - 1} , \quad (68)$$

the extremum in Eq. (67) is a local maximum. This inequality is e.g. satisfied when $r = 1, s = 100$ and $k^2 = 1.5$ as shown in Fig. 12 (thick solid curve). The local maximum in this case is $\rho_a^{extr} = 205/(2\sqrt{452}) \approx 4.82$. Moreover, when Eq. (68) is satisfied the ratio $\rho_a(t)$ has two other extrema as well. These extrema are global minima and occur when

$$gt\sqrt{k^2 - 1} = \pm \arcsin \left[\sqrt{(k^2 - 1) \frac{r}{s - r + 1}} \right] + n_{\pm}\pi , \quad (69)$$

where $n_+ = 0, 1, 2, 3, \dots$ and $n_- = 1, 2, 3, \dots$. The particular value of this minimum is

$$\rho_a^{min} = 2 \sqrt{\frac{1 + 1/s}{2 + 1/r + 1/s + 1/(rs)}} \quad , \quad (70)$$

independent of the detuning parameter k^2 . The minimum value corresponding to the thick solid curve in Fig. 12 is $\rho_a^{min} = 2\sqrt{101/302} \approx 1.16$.

If, on the other hand, Eq. (68) is violated then ρ_a^{extr} in Eq. (67) is the only extremum. It is a global maximum when $r = 0$ (see e.g. thick solid curve in Fig. 11) and a global minimum when $r \neq 0$ (see e.g. thin solid curve in Fig. 12). In both cases the global extremum is given by Eq. (67).

When the system is initially in a coherent state the signal-to-noise ratio is essentially the same as in the Fock case. The essential difference is that $\rho_a(t)$ is finite at the revival times since the variance is not zero.

An alternative definition of the signal-to-noise ratio can be obtained by considering the quadrature operator

$$X_a(t) = \frac{1}{\sqrt{2}} U_I^\dagger [a + a^\dagger] U_I \quad , \quad (71)$$

where U_I is the time-evolution operator in Eq. (10). The signal-to-noise ratio is then defined by

$$\eta_a(t) = \frac{\langle X_a(t) \rangle^2}{Var[X_a(t)]} \quad . \quad (72)$$

From this definition we immediately see that $\eta_a(t) = 0$ for a Fock state. Eq. (72) is, however, non-trivial for a coherent state $|\alpha\rangle_a \otimes |\beta\rangle_b \equiv |\alpha, \beta\rangle$. In this case the ratio $\eta_a(t)$ is

$$\eta_a(t) = \frac{K(t) + x(t) \{ |\alpha|^2 - 2\text{Re}[\alpha\beta A_-(t)] + |\beta|^2 y(t) \}}{n_0(t) + 1/2} \quad , \quad (73)$$

where

$$K(t) \equiv \text{Re} [e^{-2A_0^*(t)} (\alpha - \beta^* A_-^*(t))^2] \quad . \quad (74)$$

The functions $x(t)$, $y(t)$ and $n_0(t)$ are given by Eq. (33), Eq. (34) and Eq. (35), respectively. The signal-to-noise ratio in Eq. (73) cannot take on any value: it has an upper bound. According to Yuen [36] the maximum signal-to-noise ratio obtainable for the (two-photon) coherent state $|\alpha, \beta\rangle$ cannot exceed the value $4\langle n_a(t) \rangle [\langle n_a(t) \rangle + 1]$, i.e.

$$\eta_a(t) \leq 4\langle n_a(t) \rangle [\langle n_a(t) \rangle + 1] \quad , \quad (75)$$

where $\langle n_a(t) \rangle = \langle \beta, \alpha | a^\dagger(t) a(t) | \alpha, \beta \rangle$. It is natural to ask for what values of α , β and k^2 can we reach this optimal Yuen-limit? As an illustrative example we choose a large k^2 ,

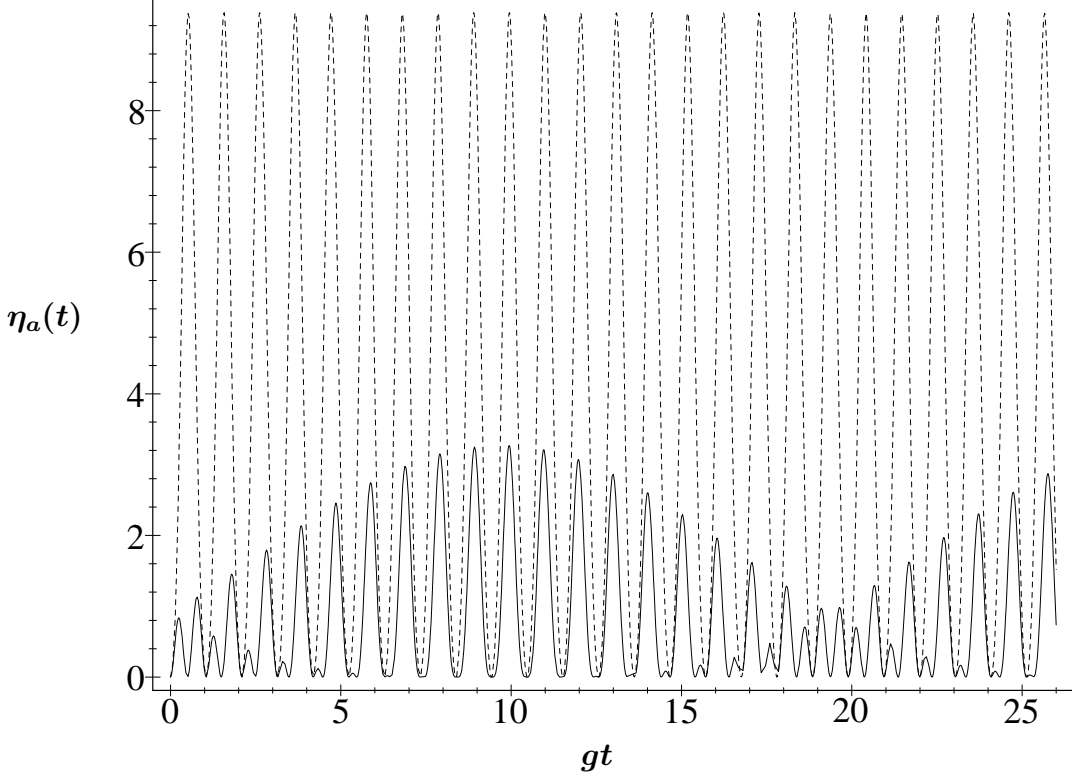


Figure 13: The signal-to-noise ratio $\eta_a(t)$ when $k^2 = 10$. The system is initially in the coherent state $|\alpha, \beta\rangle$ where $\alpha = 0$ and $\beta = 3$ (solid curve). The dotted curve is the corresponding Yuen-limit.

e.g. $k^2 = 10$, and $\alpha = 0$ and $\beta = 3$. The result of a numerical calculation is shown in Fig. 13. As we can see from such a calculation, there is approximately a factor of 2.5 in difference between the maximum $\eta_a(t)$ -value (solid curve) and the optimal Yuen-limit (dotted curve). In other words, the signal is not very far from its optimal value. The price we have to pay to come this close to the optimal Yuen-limit is the low value of $\eta_a(t)$ itself. If we, on the other hand, choose a small k^2 , e.g. $k^2 = 1.5$ (with the same α and β), the physics is different. The maximum ratio $\eta_a(t)$ is then $\mathcal{O}(10^1)$, which means that the signal is strong as compared to the noise. In this case the Yuen-limit is, however, $\mathcal{O}(10^3)$, so $\eta_a(t)$ is very far from the optimal Yuen-value. Numerical studies suggest that these observations are quite generic.

8 Final Remarks

By means of an, in general time-dependent, Bogoliubov transformation or what is

called a two-mode squeeze operator $S(z)$ in quantum optics [11], given by

$$S(z) = \exp(z^*ab - za^\dagger b^\dagger) \quad , \quad (76)$$

where $z = r \exp(i\phi)$, one can diagonalize the Hamiltonian Eq. (9) instantaneously in terms of the canonical operators

$$\begin{aligned} A(z) = S(z)aS^\dagger(z) &= a \cosh r + b^\dagger \exp(i\phi) \sinh r \quad , \\ B(z) = S(z)bS^\dagger(z) &= b \cosh r + a^\dagger \exp(i\phi) \sinh r \quad . \end{aligned} \quad (77)$$

With the choice Eq. (12) we e.g. find that

$$H = \Omega_A A^\dagger(z)A(z) + \Omega_B B^\dagger(z)B(z) + \Omega_0 \quad (78)$$

where

$$\begin{aligned} \Omega_A &= \omega_- + \omega_+ \sqrt{1 - g^2/\omega_+^2} \quad , \\ \Omega_B &= -\omega_- + \omega_+ \sqrt{1 - g^2/\omega_+^2} \quad , \\ \Omega_0 &= \omega_+ \sqrt{1 - g^2/\omega_+^2} \quad , \end{aligned} \quad (79)$$

and where $\omega_\pm = (\omega_a \pm \omega_b)/2$. The squeeze parameters are given by

$$\cosh(2r) = 1/\sqrt{1 - g^2/\omega_+^2} \quad , \quad \phi = \frac{\pi}{2} - \omega t \quad . \quad (80)$$

The diagonalization procedure above is well-defined as long as $g^2 < \omega_+^2$. If, on the other hand, $g^2 > \omega_+^2$ then the instantaneous eigenvalues Ω_A and Ω_B become complex. This indicates an instability in the system. As we have seen in the present paper, one can explicitly solve the time-dependent Schrödinger equation in such a situation and, as we have seen above, the physics of the instability actually manifest itself in an exponentially increasing particle, i.e. photon, production. In the case $k^2 < 1$ we have also seen that the asymptotic time-limit of the reduced systems can be described by thermal distributions. In general the distributions are not identical (see e.g. Eqs.(39) and (40)). But, nevertheless, if the initial state is a pure state, the reduced entropies are the same (see Refs.[33, 34, 35]) and the entropy of the whole system is, of course, zero.

Some features of the simple model of parametric down-conversion as studied in the present paper also enters in models considered in quantum cosmology as e.g. the phenomena of non-adiabatic transitions (see e.g. Ref.[37]). To the extent that such an analogy

holds we can therefore simulate some aspects of such models in the laboratory by means of non-linear quantum optics.

ACKNOWLEDGEMENT

We are greatful to K. Olaussen and A. Zeilinger for useful correspondence. The research has been supported in part by the Research Council of Norway under contract no. 118948/410. We are greateful to our colleagues at NTNU and in particular K. Olaussen for their interets in our work.

References

- [1] M.F. Bocko and R. Onofri, “*On the Measurement of a Weak Classical Force Coupled to a Harmonic Ocsillator: Experimental Progress*”, Rev. Mod. Phys. **68** (1996) 755.
- [2] B.-S. Skagerstam, in “*Coherent States: Past, Present, and Future*”, Proceedings of the Oake Ridge 1993 International Symposium, Eds. D.H. Feng, J.R. Klauder and M.R. Strayer (World Scientific, Singapore, 1994).
- [3] W.H. Louisell, A. Yariv and A.E. Siegmann, “*Quantum Fluctuations and Noise in Parametric Processes. I.*”, Phys. Rev. **124** (1961) 1646.
- [4] J.P. Gordon, W.H. Louisell and L.R. Walker, “*Quantum Fluctuations and Noise in Parametric Processes. II.*”, Phys. Rev. **129** (1963) 481.
- [5] B.R. Mollow and R.J. Glauber, “*Quantum Theory of Parametric Amplification. I.*”, Phys. Rev. **160** (1967) 1076 and “*Quantum Theory of Parametric Amplification. II.*”, *ibid.*, **160** (1967) 1097.
- [6] B.R. Mollow, “*Quantum Statistics of Coupled Oscillator Systems.*”, Phys. Rev. **162** (1967) 1256.
- [7] D.F. Walls and M.D. Reid, “*Quantum Effects in Optics*”, Acta Physica Austriaca **56** (1984) 3.
- [8] S.M. Barnett and P.L. Knight, “*Thermofield Analysis of Squeezing and Statistical Mixtures in Quantum Optics.*”, J. Opt. Soc. Am. **B2** (1985) 467.

- [9] S.M. Barnett and P.L. Knight, “*Squeezing in Correlated Quantum Systems.* ”, J. Mod. Opt. **34** (1987) 841.
- [10] C.A. Holmes, G.J. Milburn and D.F. Walls, “*Photon-Number-State Preparation in Non-Degenerate Parametric Amplification* ”, Phys. Rev. **39** (1989) 2493.
- [11] C.M. Caves and B.L. Shumaker, “*New Formalism for Two-Photon Quantum Optics. I. Quantum Phases and Squeezed States.* ”; Phys. Rev. **A31** (1985) 3068; “*New Formalism for Two-Photon Quantum Optics. II. Mathematical Foundation and Compact Notation.* ”, *ibid.* **A31** (1985) 3093; B.L. Shumaker, “*Quantum Mechanical Pure States with Gaussian Wave Functions* ”, Phys. Rep. **135** (1986) 317.
- [12] Arvind, B. Dutta, N. Mukunda and R. Simon, “*Two-Mode Quantum Systems: Invariant Classification of Squeezing Transformations and Squeezed States* ”, Phys. Rev. **A52** (1995) 1609; C. Brief, “*Two-Photon Algebra Eigenstates: A Unified Approach to Squeezing* ”, Ann. Phys. **251** (1996) 180.
- [13] A. Yariv, “*Quantum Electronics* ” (Wiley, New York, 1967).
- [14] D.F. Walls and G.J. Milburn, “*Quantum Optics* ” (Springer, 1995).
- [15] L. Mandel and E. Wolf, “*Optical Coherence and Quantum Optics* ” (Cambridge University Press, 1995) .
- [16] M.O. Scully and M.S. Zubairy, “*Quantum Optics* ” (Cambridge University Press, 1996) .
- [17] V. Bargmann, “*Irreducible Unitary Representations of the Lorentz Group* ”, Ann. Math. **48** (1947) 568; A. Barut and C. Fronsdal, “*On Non-Compact Groups. II. Representations of the 2+1 Lorentz Group.* ”, Proc. Roy. Soc. **A287** (1965) 532; A. Barut and C. Phillips, “*Matrix Elements of Representations of Non-Compact Groups in a Continuous Basis.* ”, Commun. Math. Phys. **8** (1968) 52.
- [18] J. Wei and E. Norman, “*Lie Algebraic Solution of Linear Differential Equations* ”, J. Math. Phys. **4** (1963) 575.
- [19] G. Dattoli, S. Solimento and A. Torre, “*Algebraic Time-Ordering Techniques and Harmonic Oscillator With Time-Dependent Frequency* ”, Phys. Rev. **A34** (1986) 2646.

- [20] M. Zahler and Y. Ben Aryeh, “*Photon Number Distribution of Detuned Squeezed States*”, Phys. Rev. **A43** (1991) 6368 and “*Photon Number Distribution of Detuned Two-Mode Vacuum and Excited Squeezed States*”, Phys. Rev. **A45** (1992) 3194.
- [21] D.N. Klyshko, “*Scattering of Light in a Medium With Nonlinear Polarizability*”, Sov. Phys. JETP **28** (1969) 522 and “*Photons and Nonlinear Optics*” (Gordon and Breach, New York, 1988) .
- [22] R. Ghosh, C.K. Hong, Z.Y. Ou and L. Mandel, “*Interference of Two Photons in Parametric Down Conversion*”, Phys. Rev. **A 34** (1986) 1428.
- [23] Z.Y. Ou, L.J. Wang and L. Mandel, “*Vacuum Effects on Interference in Two-Photon Down Conversion*”, Phys. Rev. **A 40** (1989) 1428.
- [24] A. Joobeur, B.E.A. Saleh and M.C. Teich, “*Spatiotemporal Coherence Properties of Entangled Light Beams Generated by Parametric Down-Conversion*”, Phys. Rev. **A 50** (1994) 3349.
- [25] A. Joobeur, B.E.A. Saleh, T.S. Larchuk and M.C. Teich, “*Coherence Properties of Entangled Light Beams Generated by Parametric Down-Conversion and Experiment*”, Phys. Rev. **A 53** (1996) 4360.
- [26] M.H. Rubin, D.N. Klyshko, Y.H. Shih and A.V. Sergienko, “*Theory of Two-Photon Entanglement in Type-II Optical Parametric Down-Conversion*”, Phys. Rev. **A 50** (1994) 5122.
- [27] P.W. Milonni, H. Fearn and A. Zelinger, “*Theory of Two-Photon Down-Conversion in the Presence of Mirrors*”, Phys. Rev. **A 53** (1996) 4556.
- [28] A. Casado, A. Fernandez-Rueda, T. Marshall, R. Risco-Delgado and A. Zelinger, “*Fourth-Order Interference in the Wigner Representation for Parametric Down-Conversion Experiments*”, Phys. Rev. **A 55** (1997) 3879.
- [29] W.P. Grice and I.A. Walmsley, “*Spectral Information and Distinguishability in Type-II Down-Conversion with a Broadband Pump*”, Phys. Rev. **A56** (1997) 1627.
- [30] A. Mufti, H.A. Schmitt and M. Sargent, “*Finite-Dimensional Matrix Representations as Calculation Tools in Quantum Optics*”, Am. J. Phys. **729** (1993).

- [31] I.Sh. Averbukh and N.F. Perelman, “*The Dynamics of Wave Packets of Highly-Excited States Atoms and Molecules*”, Sov. Phys. Usp. **34** (1991) 572 and P.W. Milonni and S. Singh, “*Some Recent Developments in the Fundamental Theory of Light*”, in “*Advances in Atomic, Molecular, and Optical Physics*”, Eds. Sir D. Bates and B. Benderson (Academic Press, 1991).
- [32] J.R. Klauder and B.-S. Skagerstam, “*Coherent States-Applications in Physics and Mathematical Physics*”, (World Scientific, Singapore, 1985 and Beijing 1988).
- [33] H. Araki and E.H. Lieb, “*Entropy Inequalities*”, Commun. Math. Phys. **18** (1970) 160.
- [34] S.J.D. Phoenix and P.L. Knight, “*Fluctuations and Entropy in Models of Quantum Optical Resonance*”, Ann. Phys. (N.Y.) **186** (1988) 381 and “*Establishment of an Entangled Atom-Field State in the Jaynes-Cummings Model*”, Phys. Rev. **A44** (1991)
- [35] S.M. Barnett and S.J.D. Phoenix, “*Entropy as a Measure of Quantum Correlations*”, Phys. Rev. **A40** (1989) 2404.
- [36] H.P. Yuen, “*States That Give the Maximum Signal-to-Noise Ratio for a Fixed Energy*”, Phys. Lett. **A56** (1976) 180. Also see Y. Feng and A.I. Solomon, “*Optimal Signal-to-Quantum Noise Ratio for Nonclassical Number States*”, quant-ph/9712020.
- [37] S. Massar and R. Parentani, “*Particle Creation and Non-Adiabatic Transitions in Quantum Cosmology*”, Nucl. Phys. **B513** (1998) 375.